LARGE EDDY SIMULATION OF WIND LOADS ON A LOW-RISE STRUCTURE AND COMPARISON WITH WIND TUNNEL RESULTS

Isam Janajreh, *ijanajreh@masdar.ac.ae* Mechanical Engineering Program, Masdar Institute of Science and Technology, Abu Dhabi, United Arab Emirates

Ilham Talab, *italab@masdar.ac.*ae Mechanical Engineering Program, Masdar Institute of Science and Technology, Abu Dhabi, United Arab Emirates

Emil Simiu, *emil.simiu@nist.gov* National Institute of Standard and Technology, Gaithersburg, USA

ABSTRACT

This work presents estimates of time histories of pressure coefficients at several taps on the roof of a 1/200 model of a 200 x 100 x 20 ft low-rise building with a 1/24 slope gable roof building. The estimates were obtained using a large eddy simulation (LES). The first and second moments as well as peaks for the time histories are compared with those obtained in boundary layer wind-tunnel measurements at the University of Western Ontario. Mean pressures compared reasonably well with the corresponding wind tunnel measurements while peak values were underestimated significantly. The current computations resulted in a T.I. near 0.05, less than half the value reported for the wind tunnel. Practically T.I provoked with the presence of spires and roughness elements whereas numerically is imposed on the incoming mean flow via spectral syntheses. It is noted that the computation times required to obtain records of length comparable to wind tunnel records are, at present, prohibitively large.

Keywords: Aerodynamics, Computational Fluid Mechanics (CFD), Large Eddy Simulation, Wind Engineering

1. INTRODUCTION

Computational Fluid Dynamics (CFD) is expected to become a viable tool for obtaining aerodynamic data that can be used confidently for structural design. In recent years, higher resolution schemes and faster solver algorithms have been developed, including, multi-grid solution accelerators, higher order special discretization algorithms, and arbitrary Lagrangian-Eulerian formulation. Computational hardware advances, i.e., augmentation in processor speed, improvements in parallel computation and digital storage capabilities, are important steps toward making CFD an increasingly useful tool. However, wind engineering applications continue to pose a challenge to CFD owing to the difficulty of modeling turbulence in the atmospheric boundary layer and in regions around bluff bodies where wake flows, flow separation and reattachment, vortex shedding, and free shear layers occur. Transient

flows render data processing and management an even more difficult task. Reynolds Average Navier-Stokes (RANS) turbulence models have demonstrated their efficiency and accuracy when applied to isotropic turbulent flow fields. Their usefulness, however, is not established for application to flows around bluff bodies embedded within the atmospheric boundary layer. RANS turbulence treats both large- and small-scale turbulence similarly. Theory and experiments, in contrast, suggest that only the small turbulent scales are universal (i.e., independent of boundary conditions). This is an important limitation of RANS. Direct Numerical Simulation (DNS) and Large Eddy Simulations (LES) are alternatives, albeit costly, to RANS that can model satisfactorily the low frequency scales. Temporal and spatial resolutions, down to the viscous dissipation scale, i.e., the Kolmogorov scale are given by:

$$\eta = L.\mathrm{Re}^{-3/4} \tag{1}$$

where L is the characteristic length of the flow and Re is the Reynolds number, would place high demands on DNS, since to solve the flow field down to this high resolution scale the required number of nodes for one dimension would be $Re^{3/4}$; and $Re^{9/4}$ for three dimensions. For the problem at hand where Re = 38,100, the corresponding number of nodes is $1.23\text{x}10^{10}$, which is intractable given the current computational capabilities. Therefore, DNS is primarily useful for understanding the turbulence physics at low Reynolds numbers and gaining insight into the development and assessment of turbulence closure models. The calculations must accommodate both the large scales that are imposed by external effects and the small scale associated with viscous dissipation. LES uses the equations of motion of the flow to model its large scale motions. However, unlike DNS, scales comparable to or smaller than the grid size are modeled by implementing a universal turbulence model. In wind tunnels, large upstream spires and roughness fetches create turbulent flows that simulate the atmospheric boundary layer flow with various degrees of success. As comparisons between results obtained by various wind tunnel laboratories show, such simulations are difficult to achieve, particularly at low elevations of interest for low-rise building design (see, Fritz et al., 2008, Main and Fritz, 2000).The simulated pressure records are typically stored as nondimensional pressure coefficients (i.e. $C_p(t) = p(t)/0.5\rho V^2$, where $p(t)$ denotes the recorded pressure, ρ denotes the fluid density, and V denotes the mean velocity in the undisturbed upstream flow at a specified reference height. The sampling frequency f for the model and the prototype are related as follows:

$$(Hf/V)_m = (Hf/V)_p \quad or \quad f_m = \lambda f_p V_m/V_p \tag{2}$$

where H denotes the characteristic length (e.g., the building height), f denotes the sampling frequency, and V denotes the mean wind velocity at the reference height; λ represents the scale ratio, and the subscripts m and p represent model and prototype scales, respectively. Records on the order of one minute are typical for wind tunnel tests. Owing to current computational limitations, in this work shorter records will be obtained. Such shorter records can be useful for research purposes, even though the sampling errors inherent in them can be relatively large (Sadek et al. 2004).

Solving for 1-s long, the pressure time record for the 1/200 model comprising a 1,200,000 finite volume cell requires 8 to 6 weeks period utilizing a quad 2.4GHz processor. The sampling time and solution stability are constrained by the dilation wave speed via the Courant-Friedrichs-Lewy (CFL) condition (Adina, 2006), that is, $CFL \equiv \Delta t . V_H / \min(dx, dy, dz) \leq 1$, where Δt is the time step, V_H is the local flow speed, and *dx*, *dy* and *dz* are the cell dimensions. The desired residual values for continuity and momentum are 10^{-6} and 10^{-8} respectively.

2. OBJECTIVES

This work consists of computing and generating pressure time histories at points located on the building roof, and carrying out comparisons with corresponding pressure tap data obtained at the Boundary Layer Wind Tunnel Laboratory of the University of Western Ontario (Ho et al.,2005). The objective is to assess the feasibility of LES calculations to study bluff body aerodynamics induced by atmospheric boundary-layer flow over low-rise structures. The simulations require the construction of an appropriate LES resolution mesh around a 1/200 model of the building. The domain is discredited by using blocks with a hexagonal cell type to allow more accurate calculations of momentum and mass exchange with the surrounding cells. Walls are padded with a surface boundary layer to capture the high velocity gradients near their surface. Velocity profiles are computed at several stations upstream and downstream of the building. Building pressure coefficient contours maps are also developed. The flow field around a low-rise structure immersed in the atmospheric boundary layer is characterized by the presence of stagnation regions, standing vortices, separation, reattachment, von Karman's vortex street, and a pronounced wake as shown in Fig. 1. The flow is turbulent, non-homogeneous and anisotropic. The common eddy viscosity models of the $\kappa-\varepsilon$ and $\kappa-\omega$ type overestimate turbulence production near the separation regions (Murakami, 1992) and very diffusive that dilutes an accurate prediction of separation and surface pressure.

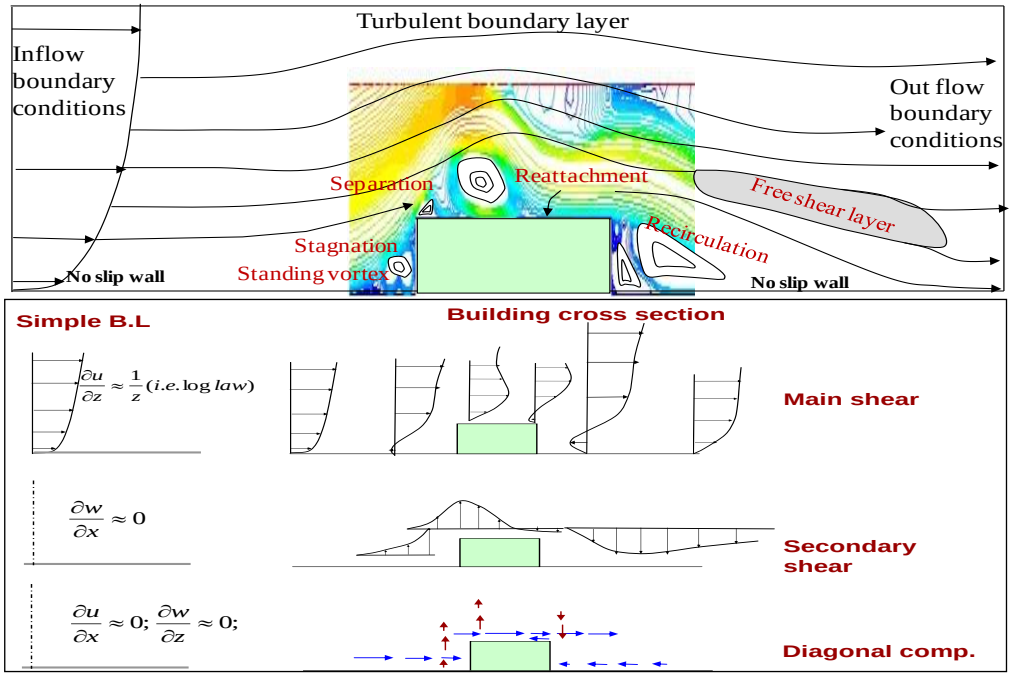

Figure 1. Characteristic of the Flow around Low Rise Structure.

3. GOVERNING SYSTEM OF EQUATIONS

The Navier-Stokes equations which govern the flow are statements of conservation of mass (continuity), and momentum. Expressing fluctuating quantities as sums of a mean and a perturbation term, $\phi_i(\vec{x},t) = \bar{\phi}_i(\vec{x},t) + \phi'_i(\vec{x},t)$), and using time averaging, these equations, to which constitutive relations between stresses and displacements or derivatives are applied, are written as:

$$Continuity: \quad \frac{\partial \bar{\rho}\bar{u}_i}{\partial x_i} = 0 \tag{3}$$

$$Momentum: \quad \frac{\partial \bar{\rho}\bar{u}_i}{\partial t} + \frac{\partial}{\partial x_j}(\bar{\rho}\bar{u}_j\bar{u}_i) = \frac{\partial \tau_{ij}}{\partial x_j} + \bar{\rho}g \tag{4}$$

$$Constitutive: \quad \tau_{ij} = -\bar{p}\delta_{ij} + \mu\left(\frac{\partial \bar{u}_i}{\partial x_j} + \frac{\partial \bar{u}_j}{\partial x_i}\right) - \bar{\rho}\,\overline{u'_i u'_j} \tag{5}$$

where t = time advancement, x_i = Cartesian coordinate (i = 1,2,3), u_i = velocity component in x_i direction, ρ = density, g_i = gravitational acceleration component in x_i direction, τ_{ij} = stress tensor components, p = pressure, μ = molecular viscosity, u'_i = velocity fluctuations about ensemble average velocities. The over bar denotes the ensemble averaging process. The $\overline{u'_i u'_j}$ term due to turbulence is referred to as Reynolds stress. The common eddy viscosity κ–ε turbulent closure model is expressed as follows:

$$Turbulence\ closure: -\bar{\rho}\,\overline{u'_i u'_j} = \mu_t\left(\frac{\partial \bar{u}_i}{\partial x_j} + \frac{\partial \bar{u}_j}{\partial x_i}\right) - \frac{2}{3}\bar{\rho}\,k\delta_{ij} \tag{6}$$

where the μ_t is the turbulent viscosity, k is the turbulent kinetic energy, and

$$\mu_t = f_\mu \frac{C_\mu \rho k^2}{\varepsilon} \tag{6a}$$

In Eq. 6a ε is the turbulent dissipation rate, and f_μ and C_μ. are empirical constants. Substituting Eq. 6 in Eq. 5 conveniently allows adding the Reynolds stresses term to the diffusion term (second term in the right-hand side of Eq. 5), resulting in an equivalent viscosity:

$$\mu_{total} = \mu + \mu_t \tag{6b}$$

The approach described in this section is referred to as the RANS approach.

4. TURBULENT MODELING VIA LARGE EDDY SIMULATION

Unlike the RANS turbulence modeling, LES implements a simpler model and is inherently transient. It allows explicit resolution of the large-scale turbulent motion while separately modeling small-scale turbulence. The dependent flow field variables are all written in the form:

$$u_i(\vec{x},t) = \bar{u}_i(\vec{x},t) + u_i'(\vec{x},t) \tag{7}$$

where the bar indicates the resolved scale and the prime indicates the subgrid scale. The large scale field is the result of filtering the flow field with a filter kernel G(x,ζ;Δ), e.g., a Box, Gaussian, or spectral cut-off filter (Lesieur et al., 2005). The resulting flow field is expressed as follows:

$$Filter: \quad \bar{u}_i(\vec{x},t) = \int G(\vec{x},\vec{\varsigma};\Delta)\, u_i(\vec{\varsigma},t)\, d^3\vec{\varsigma} \tag{8a}$$

$$Continuity: \quad \frac{\partial \bar{\rho}}{\partial t} + \frac{\partial \bar{u}_i}{\partial \bar{x}_i} = 0 \tag{8b}$$

$$Momentum: \quad \frac{\partial \bar{u}_i}{\partial t} + \frac{\partial}{\partial x_j}(\bar{u}_i \bar{u}_j) = -\frac{1}{\rho}\frac{\partial \bar{p}}{\partial x_i} + \frac{\partial}{\partial x_j}\left(\nu \frac{\partial \bar{u}_i}{\partial x_j}\right) - \frac{\partial \tau_{ij}}{\partial x_j} \tag{8c}$$

where G is the spatial normalized ($\int G(\vec{x},\vec{\varsigma};\Delta)\, d^3\vec{\varsigma} = 1$) filter operator at $\vec{x}$ over the defined cell space of $\vec{\varsigma}$, Δ represents the bandwidth filter parameter that characterizes individual cell mesh width, and ν is the kinematics viscosity. The subgrid scale turbulent stress tensor τ_{ij} is expressed as:

$$\tau_{ij} = \bar{u}_i \bar{u}_j - \overline{u_i u_j} \tag{9}$$

The filtered Navier-Stokes equation will contain large scale terms with the overbar symbol and small scale terms with the prime symbol. The prime terms are referred to as subgrid scale terms (SGS), and will take the form of Reynolds stresses. To assure closure of the governing system of equations, the effect of the small scale velocity components needs to be modeled. At this point, SGS (τ_{ij}) is unknown and requires a turbulent closure model. The three-dimensional Smagorinsky Eddy Viscosity model is used. It implements the following linear relation between the filtered SGS tensor (τ_{ij}) and the filtered strain rate tensor (s_{ij}):

$$Turbulent\ closure: \quad \tau_{ij} = 2\nu_t s_{ij} - \frac{2}{3}\tau_{kk}\delta_{ij} \tag{10}$$

where ν_t is the turbulent kinematic viscosity, and the strain rate tensor s_{ij} is the resolved field defined as:

$$s_{ij} = \frac{1}{2}\left(\frac{\partial \bar{u}_i}{\partial x_j} + \frac{\partial \bar{u}_j}{\partial x_i}\right) \tag{11}$$

τ_{kk} is the isotropic part of the subgrid-scale stresses and is added to the filtered pressure term. The turbulent kinematic viscosity ν_t, has the dimensions LV, where L and V are a length scale and a velocity scale, respectively. Smagorinsky (1963) proposed the expression $\nu_t = c_s \Delta^2 \sqrt{s_{ij} s_{ij}}$, where Δ is the filter bandwidth, s_{ij} is the strain tensor (whose dimension is $[T]^{-1}$), and c_s is a non-dimensional factor determined experimentally. Accordingly, the turbulent kinetic energy (κ) and turbulent dissipation rate (ε) are expressed as:

$$k = c_k \Delta^2 (s_{ij} s_{ij}) \tag{12}$$

$$\varepsilon = c_\varepsilon k^{3/2} / \Delta = c_\varepsilon c_k^{3/2} \Delta (s_{ij} s_{ij})^{3/2} \tag{13}$$

respectively; where c_k and c_ε are determined experimentally. In the current implementation of finite volume discretization, the filter width is related to the mesh cell as follows: Δ=(cell volume)$^{1/3}$. Near the wall, and in order to capture and resolve the smallest turbulence scales, the filter width is adjusted to be min (0.04y, Δ) where y is the distance between the cell center and the closest wall. The dynamic Smagorinsky-Lilly model does implement a fixed value for c_s and suggests a method to derive its value dynamically from the resolved field (Holscher, 1996).

5. WIND TUNNEL PRESSURE RECORDS

The wind tunnel data considered here were reported by Ho (2005), and are available on www.nist.gov/wind. The model is equipped with over 400 pressure taps, as depicted in Fig. 2.

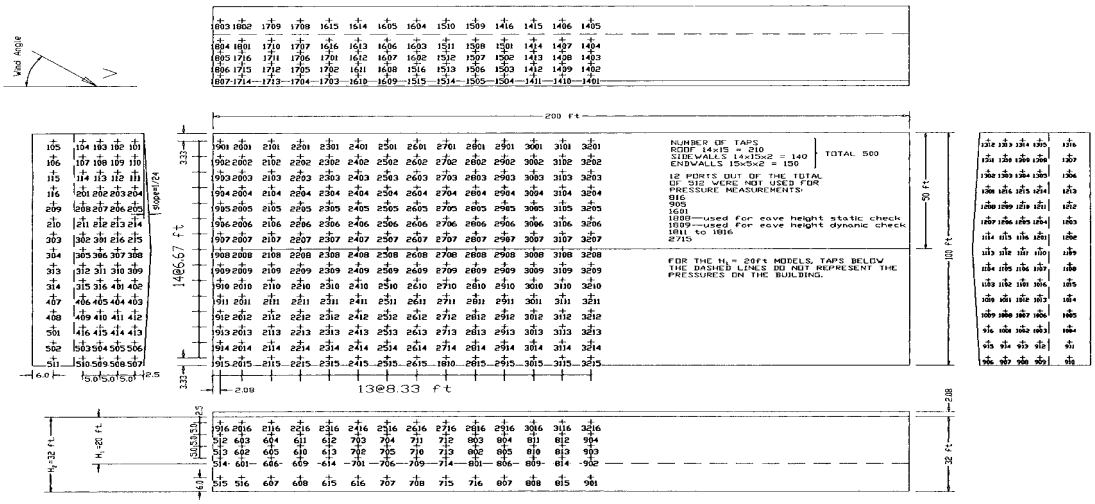

Figure 2. Pressure Taps Location with Respect to the Building Roof and along the Walls.

Pressure coefficient time histories were sampled at 400 Hz for 60 seconds and obtained at 36 wind directions between 0^{o} and 180^{o} at 5^{o} intervals by setting up the model at the center of the circular base and incrementally rotating the base. The wind tunnel test section included large spires to create wind gusts at the wind tunnel entrance, as well as roughness elements as tall as the building height *H* upstream of the building model. A shorter 0.1*H* roughness element in the vicinity of the model was used to simulate the atmospheric boundary layer. The roof pressures were obtained via a high speed pressure scanner connected to the tap tubing and then normalized via the dynamic pressure obtained at the same eave height *H* to yield pressure coefficients. The full-scale hourly wind speed was 10.15m/s and was used in the production of the wind tunnel test data. Three sets of two successive pressure taps were located at the center, the middle, and the edge of the upstream building's roof-edge. Their locations are listed in Table 1, normalized with respect to the building height H. As shown in Fig. 2, taps 1908, 1904, and 1901 are located on the leftmost row parallel to the small dimension of the building on the gable line, two horizontal rows away from the gable line, and four horizontal rows away from the gable line (i.e., near the long wall line at the top of the plan view), respectively. Taps 2008, 2004, and 2001 are located on the row next to the leftmost row parallel to the small dimension of the building on the gable line, two horizontal rows away from the gable line, and four horizontal rows away from the gable, respectively. The wind tunnel pressure coefficient time histories for three taps in the first row (taps 1908, 1904, 1901) and an additional three taps in the second row (taps 2008, 2004 and 2001) are depicted in Fig. 3.

Table 1. Location of the Data Points Considered in the Study.

Center	*x(H)*	*y(H)*	*z(H)*	**Middle**	*x(H)*	*y(H)*	*z(H)*	**Side**	*x(H)*	*y(H)*	*z(H)*
1908	0.1040	1.0651	0.0000	**1904**	0.1040	1.0304	1.3340	**1901**	0.1040	1.0043	2.3345
2008	0.5205	1.0651	0.0000	**2004**	0.5205	1.0304	1.3340	**2001**	0.5205	1.0043	2.3345

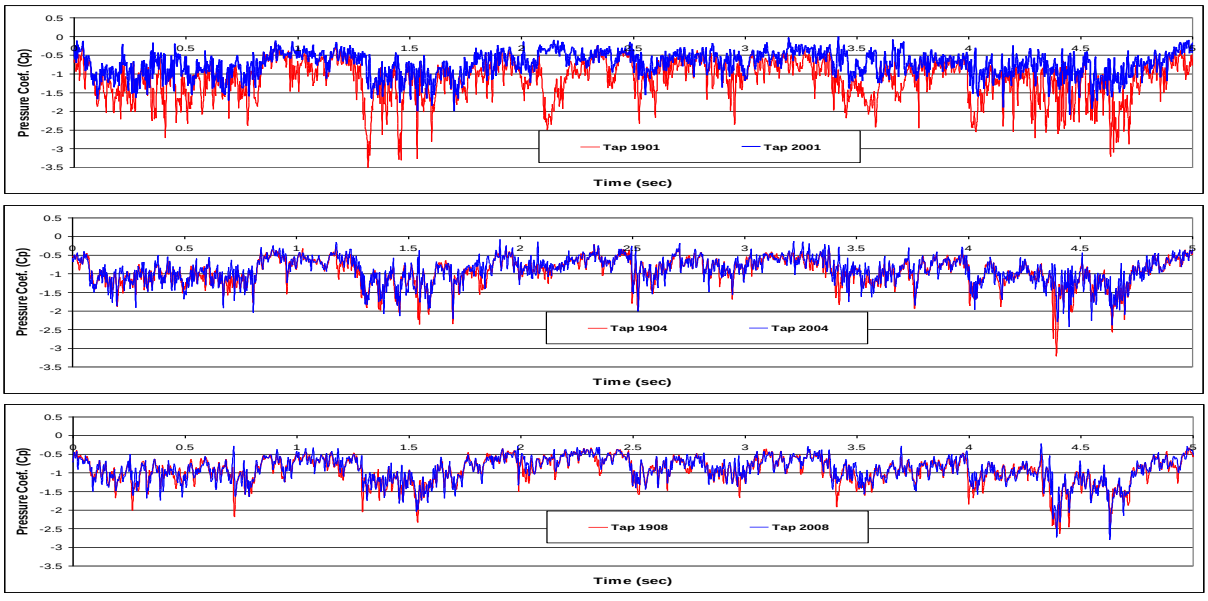

Figure 3. Wind Tunnel Time Series of Cp at Three Sets of Two Successive Roof Taps (side, quarter, center)

Only the normal incidence case (0^o, see Fig. 1) was simulated and considered for comparison. Before comparing wind tunnel measurements and computational results, the records were tested for quality (see Ho et al., 2005). Numerically simulated records on the order of 60 seconds are difficult to obtain. For this reason the individual wind tunnel records were tested by performing a stationary test. A stationary record implies that the mean and standard deviation are independent on record length. Fig. 4 depicts those sample statistics as functions of record length. Fig. 4 suggests that, within sample errors that increase with decreasing record length, a record length of a few seconds can be reasonably representative of the mean and variance of the pressure coefficients.

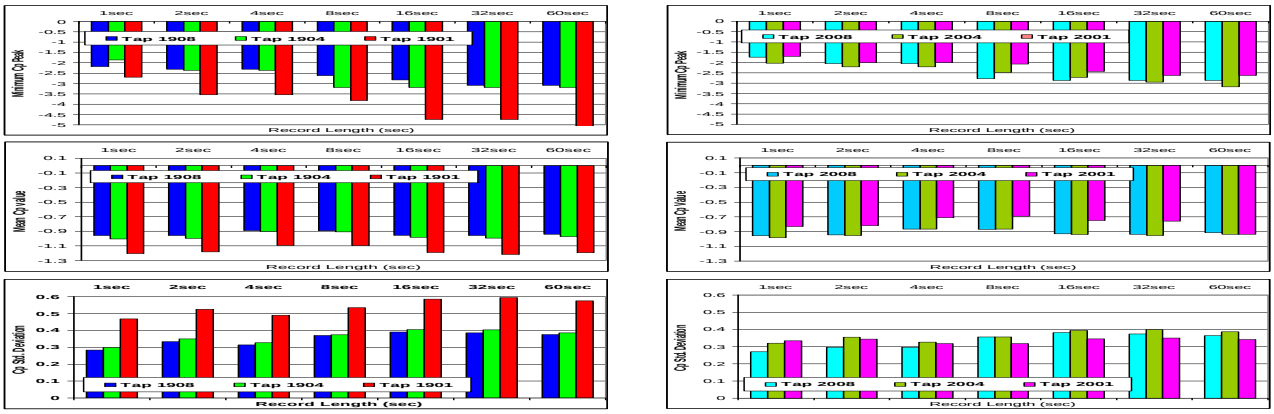

Figure 4. Wind Tunnel Records Minimum, Mean, and Variance of C_p as Function of Record Length.

6. NUMERICAL ANALYSIS

Simulation Set-up and Boundary Conditions: The computational domain is set up to simulate the flow over a 1/200 scale model of the 10*H* x 5H x *H* low-rise building with a 1/24 roof slope. *H* is the full scale building's 6.1 m (20 ft) eave height. The C_p time histories of the taps presented in Table 1 as well as the upstream velocity components at the model height *H* are monitored and recorded. The mesh was constructed with the objective of obtaining an accurate representation of the pressure coefficient time histories at the building surface.

A computational domain of 130*H* x 105*H* x 13.5*H* was constructed around the building. It is bounded by the ground surface with no-slip condition, the power law profile inlet at a distance of 20*H* upstream, the outlet pressure at 100*H* downstream of the building's leeward face, the two side slip walls at 20*H*, and the upper slip wall at 40*H* above the building. This domain is fitted with 60 structured blocks to better control the mesh size and admit the boundary-layer fine resolution. It is comprised of 1,200,000 hexagonal finite volume cells with wall refinements of 0.0075*H* smoothly staggered at 1.15 to 1.2 successive length ratios away from the walls. The overall mesh count is nearly 136x170x54 minus the building (44x50x44) and block connections. The targeted normalized wall distance is kept near 10 via several meshing attempts and analysis verifications. This level of refinement is required to capture the boundary layer separation and re-attachment. Fig. 5 depicts the computational domain fitted with the surface mesh of the building.

The inlet boundary condition (incoming shear wind flow within the atmospheric boundary layer) is that of an open terrain. It is appropriately modeled by the power law [ASHRAE, Ansys] such that:

$$u(z) = \begin{cases} U_{met}(h_{met.b.layer} / H_{met})^{\alpha_{met}} (z / h_{local.b.layer})^{\alpha_{local}} & z < h_{local.b.layer} \\ U_{met}(h_{met.b.layer} / H_{met})^{\alpha_{met}} & z \geq h_{local.b.layer} \end{cases} \quad (14)$$

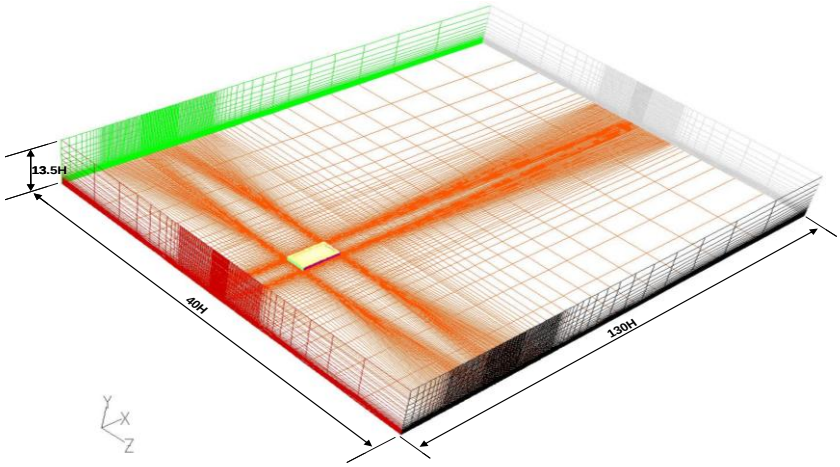

Figure 5. Computational Domain Mesh Dimensions in Building Height Units.

where U_{met} is the measured wind speed at a nearby meteorological tower site at elevation H_{met}; α_{met} and α_{local} are exponents characterizing the terrain exposure near the tower and the building; and $h_{met.b.layer}$, and $h_{local.b.layer}$ are the estimated boundary layer depths next to the tower and the building, respectively. This formula leads to a constant speed at any height *z* equal to or larger than the boundary layer depth $h_{local.b.layer}$. A typical value for the elevation of the meteorological tower H_{met} is 10m; the open terrain exponent α is taken to be 0.16; and the atmospheric boundary layer thickness *h* is assumed to be 270m. The incoming fluctuations are modeled by using a random flow generator where the flow components are computed and synthesized with a divergence-free velocity vector comprising 100 Fourier harmonics, with an initial turbulent intensity of 0.1. The assignments of the boundary conditions for the two models are summarized in Table 2 below.

Table 2. Boundary Conditions Assignment.

Boundary Region	Large Eddy Simulation (LES)
Inflow region	Velocity*: $u(z,t) = u(h_{10m})[z / h_{10}]^{0.16}$ RANS as LES start up: at I_x = 10% μ_t=10μ κ and ε are computed accordingly. -LES: Spectral synthesizer with divergence free at I_x = 10% μ_t=10μ κ and ε are computed accordingly.
Outflow region	Atmospheric pressure

Upper face of the computational domain and the far field domain	Free slip
Solid walls and ground regions	$U_1 = U_2 = U_3 = 0$: No slip, no penetration conditions

*Suggested by Simiu and Scanlan, 1996, I_x, μ_t, k, ε are turb. intensity, turb. viscosity, turb. kinetic energy, and turb. dissipation, respectively.

Numerical Results: This work implements a second-order spatial and central time scheme with a time step of $4x10^{-5}$ seconds. This time step is within the range of the Courant-Friedrichs stability requirements, particularly in the vicinity of the model, such that $CFL = \Delta t\, u_{local} / \min(\Delta x, \Delta y, \Delta z) < 3$. The normalized wall distance ($y^+ = u_w y / \nu$, where $u_w = \sqrt{\tau_w / \rho}$ and τ_w is the wall shear) is iterated in several trials of mesh construction and analysis to produce $y^+ < 10$. The achieved convergence levels for the continuity and momentum residuals were targeted to reach 10^{-6} and 10^{-8}, respectively, at each time step. The velocity pressure coupling is achieved via the SIMPLE algorithm and uses on average 30 inter-iterations per time step to reach the specified residuals. The targeted values for $y^+ < 10$ and $CFL < 3$ are verified continuously to assure the accuracy of model setup. The building drag and lift coefficients were also recorded and their history plots are used as an indicator of the stability of the computed data. These coefficients are expressed as:

$$C_l = \sum_{building\ surface} p_i\ A_{i\,lift} / (0.5\rho u^2 . A_{lift\ projected}) \tag{15a}$$

$$C_d = \sum_{building\ surface} p_i\ A_{i\,drag} / (0.5\rho u^2 . A_{drag\ projected}) \tag{15b}$$

where p_i is the computed incremental pressure applied at the incremental area A_i in the direction of the lift and drag, and A_{lift} and A_{drag} are the projected building areas in the direction of the lift and drag, respectively. Fig. 6 depicts the time history of those coefficients. It shows the flow needed 0.065 s to go through transition and become stationary. This time is equivalent to the flow "transfer time" to reach the building front ($u_{avg}(H)$=9.5m/s, L=0.6096 m). Contours of the magnitude of the velocity field at the end of 0.1736 seconds (4340th time step) are depicted in Fig. 7. They illustrate the formation of the upstream vortex core, roof separation and reattachments zone, building wake, as well as the free shear layer. The line plot of the main shear (u_x) at several locations illustrates this further. It shows the presence of a reverse flow upstream confined to the ground and extended nearly 2H length. Another reverse flow confined by the roof extends to 1.5H length. Behind the model, a mixing shear layer is formed at the edge of the wake far from the ground, and the wake roll up vortex region extends over 5H lengths.

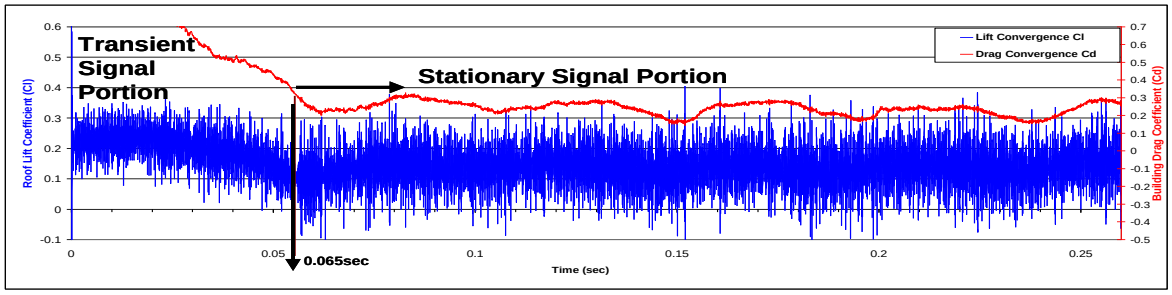

Figure 6. Results of the Global Building Lift and Drag Coefficients.

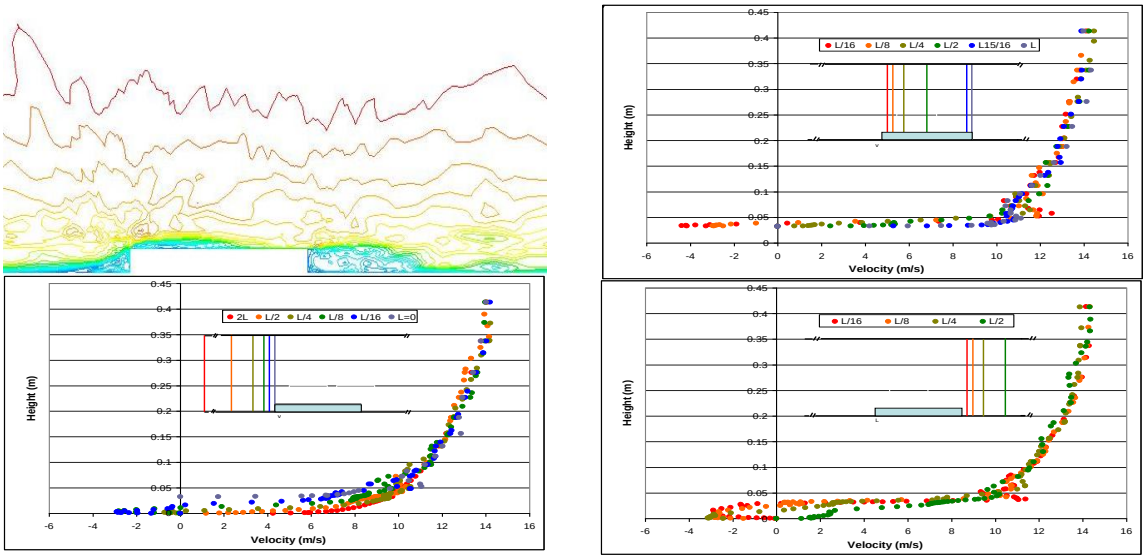

Figure 7. Computed Mean Shear Velocity at Several Locations.

Contours of the pressure coefficients and line plots on the center, the middle, and the edge are also depicted in Fig. 8; their values fall within the range obtained in the wind tunnel. Note that the stagnation region, $C_p \approx 1.0$, at the front of the building differs from the reported steady state solution and continues to be asymmetrical around the middle streamwise-vertical plane. The computed temporal velocity record at the eave elevation *H* and upstream at 10*H*, as well as the computed component spectra are depicted in Fig. 9. The energy- containing eddies are centered near 0.15 and extend to 0.35 normalized frequency, $f* = f.H/V_\infty$ where f is the frequency and V_∞ is the flow velocity. The fluctuation in the axial velocity component dominates the lateral and vertical ones.

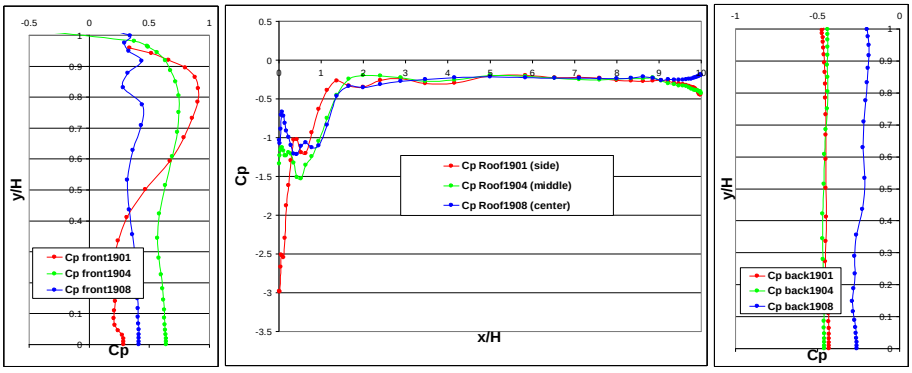

Figure 8. Pressure Coefficient Contours and Plots at the Side, Quarter and Center Lines.

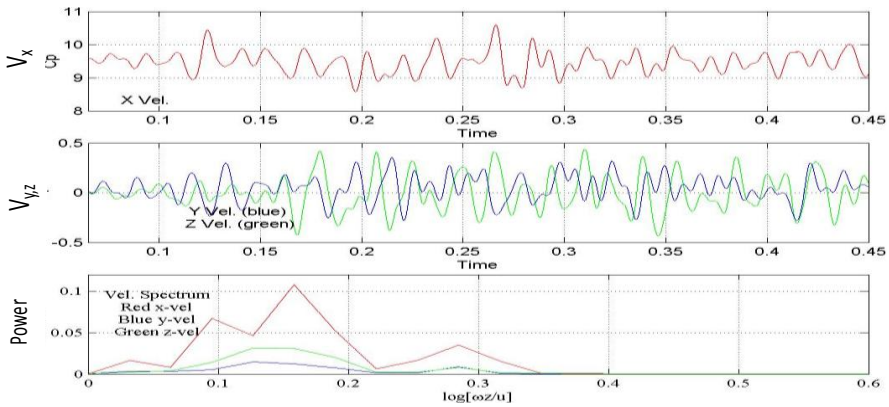

Figure 9. Computed Velocity at L Distance Upstream and at H Altitude, and Their Spectra.

The input flow velocity was perturbed via a divergence-free spectrum method to simulate incoming flow turbulence. This perturbation is captured in Fig. 9 upstream of the model; the computed local turbulent intensity is I=0.045 (Ix=0.05, Iy=0.06, Iz=0.038). The computed pressure coefficient time histories for the six taps located at center, middle, and the edge are depicted in Fig. 10, 11 and 12. For a 0.5 s computed interval, minimum, mean, standard deviation, and the number of peaks for these taps compared to the 60 s time record wind tunnel data are given in Table 3 below.

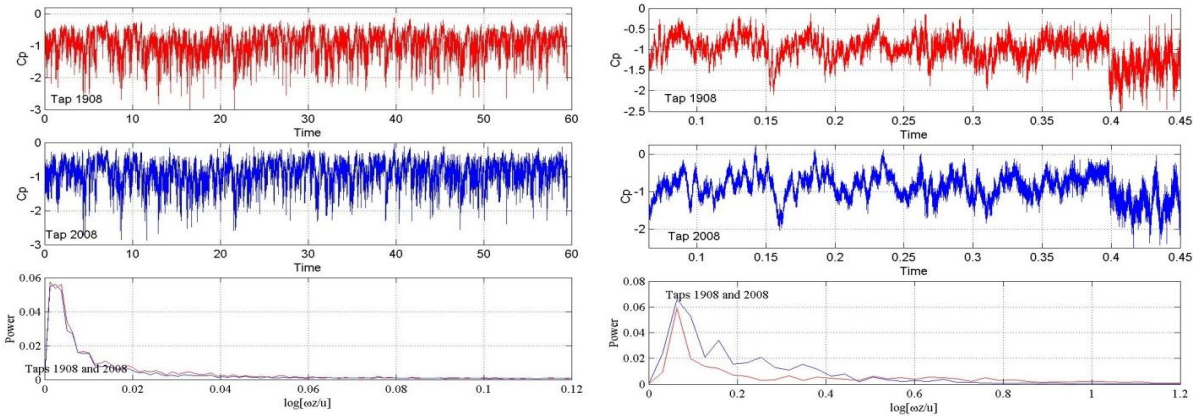

Figure 10. Wind Tunnel (Left) and Computed (Right) Time Series and Spectra Of Cp at Center Taps.

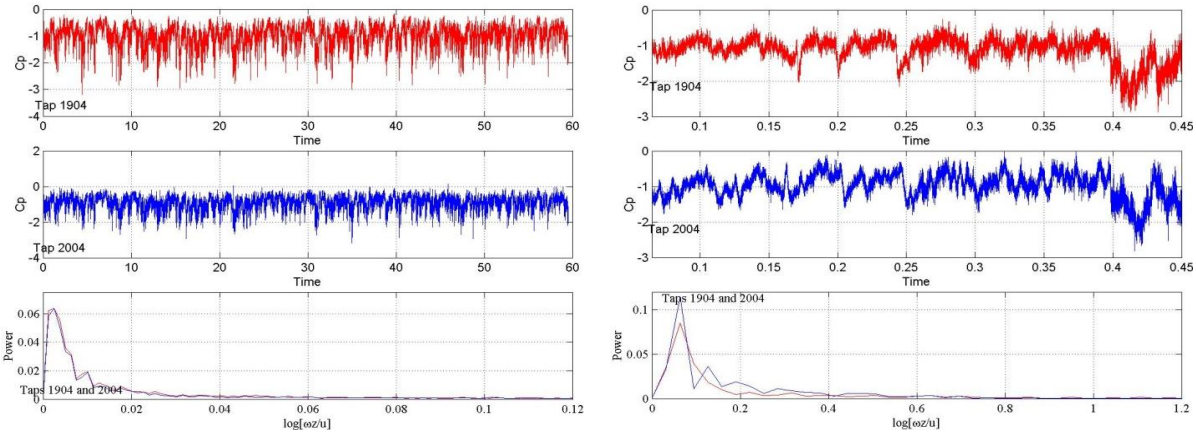

Figure 11. Wind Tunnel (Left) and Computed (Right) Time Series and Spectra of Cp at Middle Taps.

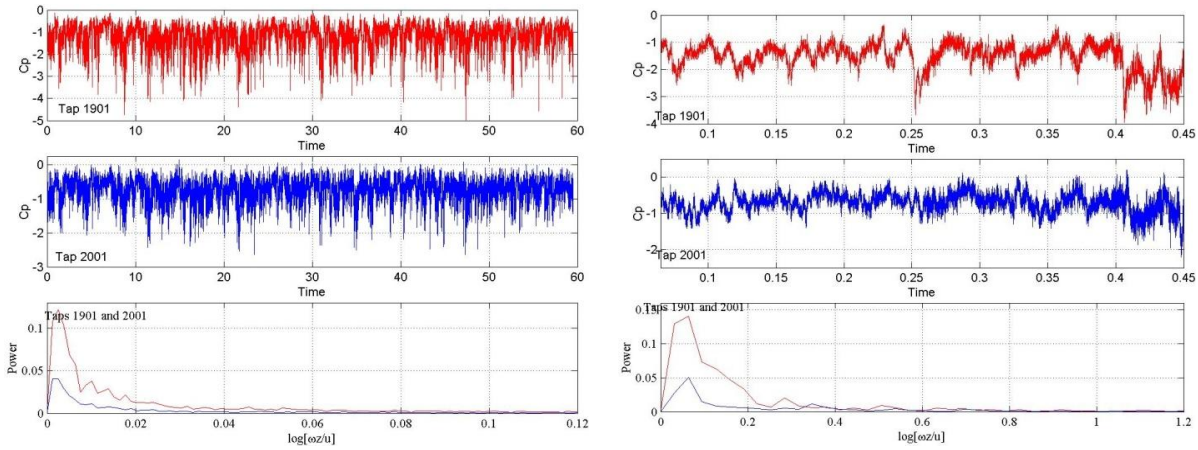

Figure 12. Wind Tunnel (Left) and Computed (Right) Time Series and Spectra of Cp at the Edge Taps.

Table 3. Minimum (min), Average (mean), and Variance Values of the Measured and Computed Cp.

Tap Num.	Min 0.5sec Comp.	Min60 sec Exp.	Avg 0.5 sec Comp.	Avg 60 sec Exp.	St. Div. 0.5sec Comp.	St. Div. 60sec Exp.	#Peaks0.5sec Comp.	#Peaks60sec Exp.
Tap 1908	-2.0897	-3.0863	-0.9393	-0.9408	0.2733	0.3756	1270	3715
Tap 2008	-2.0433	-2.8688	-0.8308	-0.9151	0.3193	0.3639	1365	3795
Tap 1904	-2.1582	-3.1894	-1.0387	-0.9742	0.2424	0.3858	1207	3678
Tap 2004	-1.7960	-3.1722	-0.9033	-0.9345	0.2810	0.3857	1466	3672
Tap 1901	-3.6773	-5.0847	-1.4027	-1.1940	0.3880	0.5741	1242	3432
Tap 2001	-1.4221	-2.6283	-0.6779	-0.9345	0.2372	0.3418	1314	4624

The data in general has similar trends as the wind tunnel data. They are normalized utilizing a fixed dynamic pressure. The velocity shows, however, a tendency to drop by 0.8% due to the turbulence introduced in the model and therefore it could produce lower instantaneous dynamic pressure. This may reduce the peak values to a level closer to those obtained in the wind tunnel. The mean values are well behaved and compare reasonably well with the wind tunnel values; a longer computed record could improve the agreement. The frequency of occurrence of peaks is important; a peak is accounted for if the pressure coefficient value drops below one standard deviation. Those numbers are compared to their counterparts obtained from the wind tunnel data at different lengths and are presented in Fig. 13. They compare favorably with records of up to 8 seconds. Fig. 14 shows a moderate mismatch between the wind tunnel axial flow profile and another resulting from the numerical simulation at one building length distance upstream. It also shows the large mismatch in the turbulent intensity which is almost 4 times higher in the wind tunnel. It is suggested that in order to improve the match between the pressure negative peaks, a higher turbulent intensity is needed for the numerical simulation. Figs. 10, 11 and 12 depict side to side comparison between pressure coefficients time histories and their frequency spectrum. The energy containing eddies frequency band extends 0.1 and 1.0 normalized frequency (i.e., 413 Hz and 3300 Hz) for the wind tunnel and numerical simulation, respectively; those eddies peak near 0.0025 and 0.05 (300 Hz and 375 Hz). Due to the low frequency resolution in the wind tunnel, the frequency values are believed to be better in the numerical simulation. The

augmentation of this intensity while achieving a tight convergence and matching the flow profile is proposed as future work.

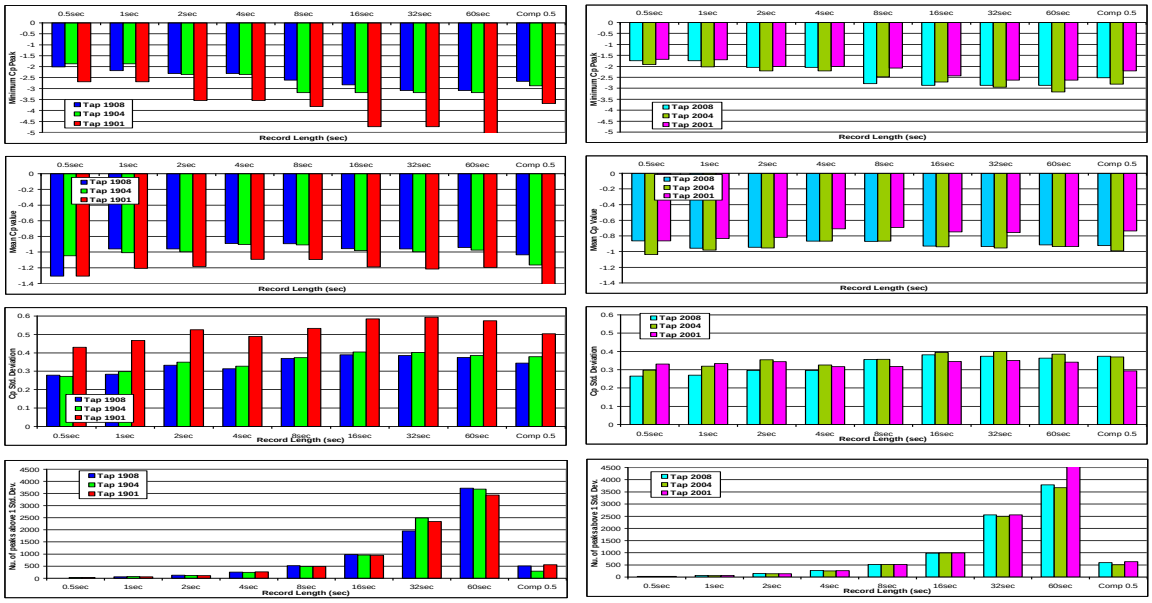

Figure 13. Wind Tunnel (left) vs. Numerical Results (right) for Avg, St. Dev. & Peaks

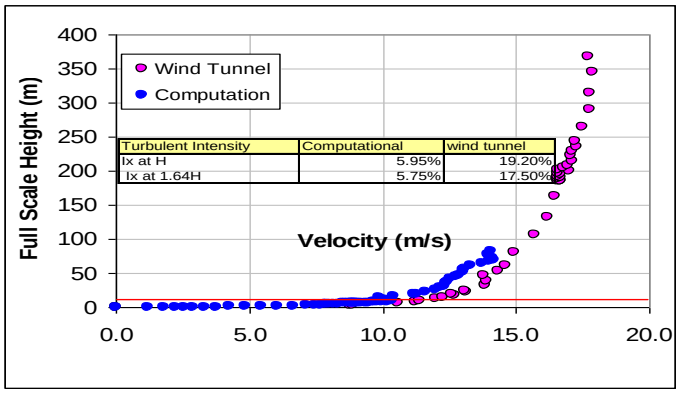

Figure 14. Numerical-Wind Tunnel Comparison for Velocity Profile and Turbulence Intensity.

7. CONCLUSIONS

This work suggests the potential feasibility of CFD utilizing Large Eddy Simulation to simulate pressure time histories obtained by wind tunnel measurements. Mean pressures compared reasonably well with the corresponding wind tunnel measurements, but peak values were underestimated significantly. The current computations resulted in a turbulent intensity near 0.05, less than half the value reported for the wind tunnel. Wind tunnel turbulence intensity is augmented by the inclusion of spires and elemental roughness. While adding spires and roughness elements in the simulation is computationally cumbersome, increasing turbulence intensities and avoid filtering it in the upstream can be achieved in the future.

This work also demonstrates the tremendous length of time required to achieve a record length equivalent to that obtained in the wind tunnel. It suggests, however, that a much shorter time record

length of a few multiples of the transfer time through the domain could be computationally feasible and adequate for some purposes, although not for design, since sampling errors inherent in such a short record could be considerable. It is also worth to mention that for stability reason which is constrained by the CFL number, the flow is subjected to a much higher sampling rate than the wind tunnel data (nearly two orders of magnitude higher than in the wind tunnel).

From this work one can estimate the CPU time and the needed computational resources to run LES simulation on low rise structures. Using the current technology, i.e. iterative, pressure based, SIMPLE solver on a domain comprising of 1,200,000, a time step of $4E^{-5}$ second was proper to attain the desired solution conversion. The simulation took 1.1 to 1.2 minutes of CPU time per time step on the quad dual 2.4GH processors (each time step took 25 to 30 inner-loop iterations to achieve the desired residuals of $1.0E^{-6}$ and $1.0E^{-8}$ for the continuity and velocity components). At a mean flow rate of 10m/s and with a constructed domain length of 130H (H is the building height at 20ft) the total transfer time nearly 0.4 second. Thus the minimum simulation CPU time necessary is nearly 62 days for one passage and 125days for two passages utilizing 4 cores. This time could be halves by increasing the number of the processor providing low latency and higher Ethernet or Infiniband core and nodes communication via MPI and pure parallel application. Commercial codes including Fluent, CFX and Star-Cd strive to offer the best linear scaling on the latest parallel architectures.

ACKNOWLEDGMENTS

The support provided by NIST and Masdar Institute for this work is highly acknowledged.

REFERENCES

Adina R & D, Inc. (2006), "Adina Theory and Modeling Guide: ARD 06-9 November 2006
Ansys, Fluent 6.3 User's Guide, and Airpack 3.0 User's Guide Fluent Inc. (2007)
ASHREA Handbook-1997 Fundamentals, American Society of Heating, Refrigerating, and Air-Conditioning Engineeris, Atlanta, Georgia, 1997.
Holscher, N. (1996), "A non-linear approach for the aerodynamic admittance of wind pressures," *Third International Colloquium on Bluff Body Aerodynamics & Applications*, July 28-August 1, 1996, Virginia Teach, Blacksburg, Virginia, pp. A VI 23-A VI 28.
Ho, T.C.E. , Surry D., Morrish D., .Kopp, G. A. (2005) "The UWO contribution to the NIST Aerodynamic database for wind loads on low building: Part 1. Archiving format and basic aerodynamic data" *Journal of Wind Engineering and Industrial Aerodynamics* 93 1-30, 2005.
Lesieur, M., Metais, O., Comte, P. (2005), "Large Eddy Simulation of Turbulence", Cambridge University Press 2005, ISBN 0-521-78124-8
Main, J. A., and Fritz, W. P. (2006), *Database-Assisted Design for Wind: Concepts, Software, and Examples for Rigid and Flexible Buildings*, National Institute of Standard and Technology Building Science Series 180, March 2006, 99 page CODEN: NBSSES.
Murakami, S., (1992), "Comparison of Various Turbulence Models Applied to a Bluff Body", 1st International Symposium on CWE, Tokyo, 1992. *J. of Wind Engineering*. No.52 Aug.
Sadek, F., Diniz, S., Kasperski, M., Gioffrè, M., , and Simiu, E., (2004), "Sampling Errors in the Estimation of Peak Wind-Induced Internal Forces in Low-Rise Structures", *J. Engrg. Mech*. Vol. 130, pp. 235-239.
Smagorinsky, J. (1963), "General Circulation Experiments with the Primitive Equations. I. The Basic Experiment", *Month. Wea. Rev.*, 91:99-164, 1963.